Electronic Supplement

Ground-Motion Variability for Ruptures on Rough Faults

Jagdish Chandra Vyas[1], Martin Galis[2,3], and Paul Martin Mai[1]

[1]King Abdullah University of Science and Technology, Saudi Arabia

[2]Comenius University, Bratislava, Slovakia

[3]Slovak Academy of Sciences, Bratislava, Slovakia

November 12, 2023

This electronic supplement contains rough-fault models depicting different realizations of fault-roughness and ground velocity waveform comparison for four rupture models at two stations. It also comprises snapshots of ground velocity at the Earth surface for A1 model, and displays shake-map like ground-motion plots that show the spatial variations of PGAs and PGVs for eighteen rupture models. Moreover, comparisons of simulated PGVs from 18 models against empirical GMMs are depicted. Additionally, it contains PGA-residual variations with respect to 18 models at 10 receivers and PGV-residuals variations at 20 stations. Finally, the PGV variability as function of different rupture style (unilateral vs bilateral) and varying amplitude of fault roughness is depicted as well.

List of figure captions

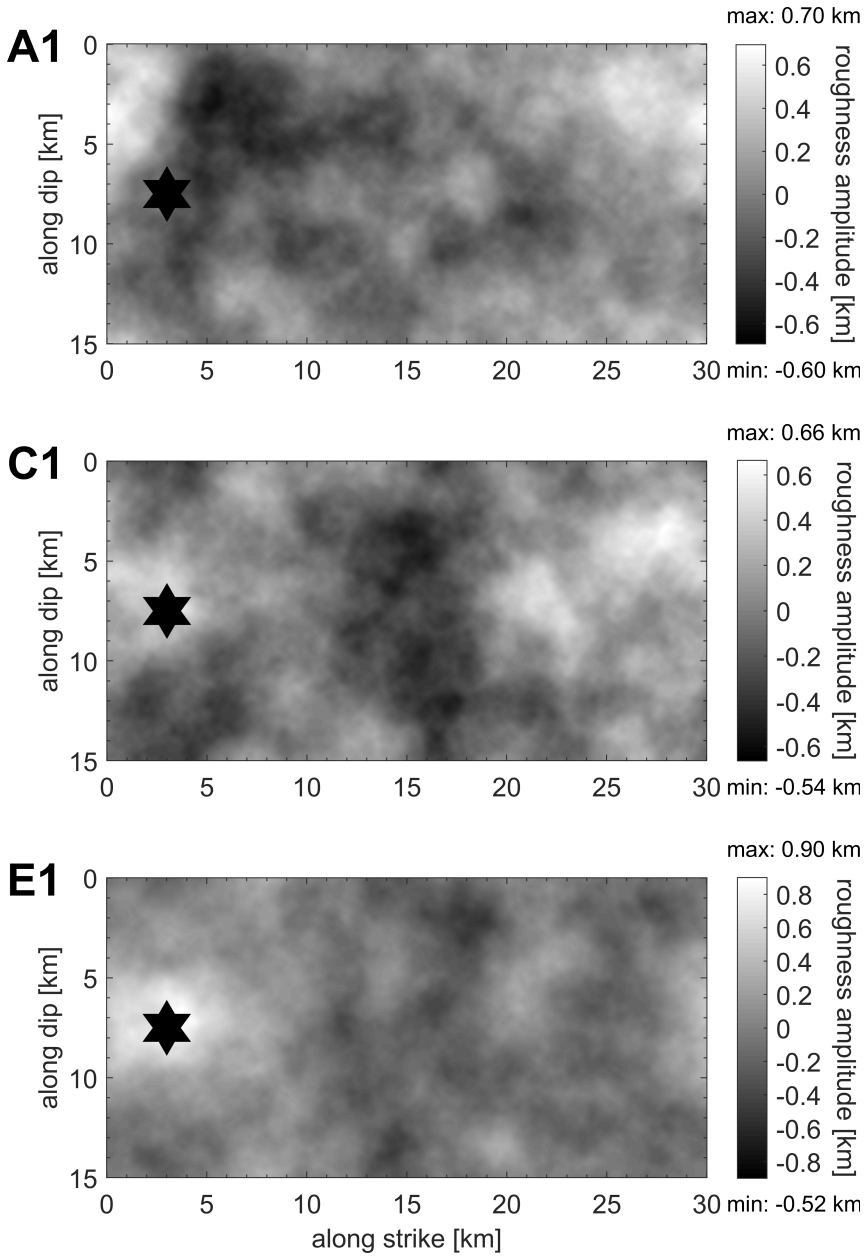

Figure S1: Comparison of three different realizations of fault roughness for models A1, C1 and E1. The black stars represent hypocenter locations. Models B1, D1i and F1 are rougher versions of models A1, C1 and E1, respectively, i.e., they share the same spatial distribution of roughness but with different height. We recall that, for example, models A2 and A3 are periodic shifts of roughness distribution of A1 model so that the hypocenter is in the middle or near the right end of the fault, respectively.

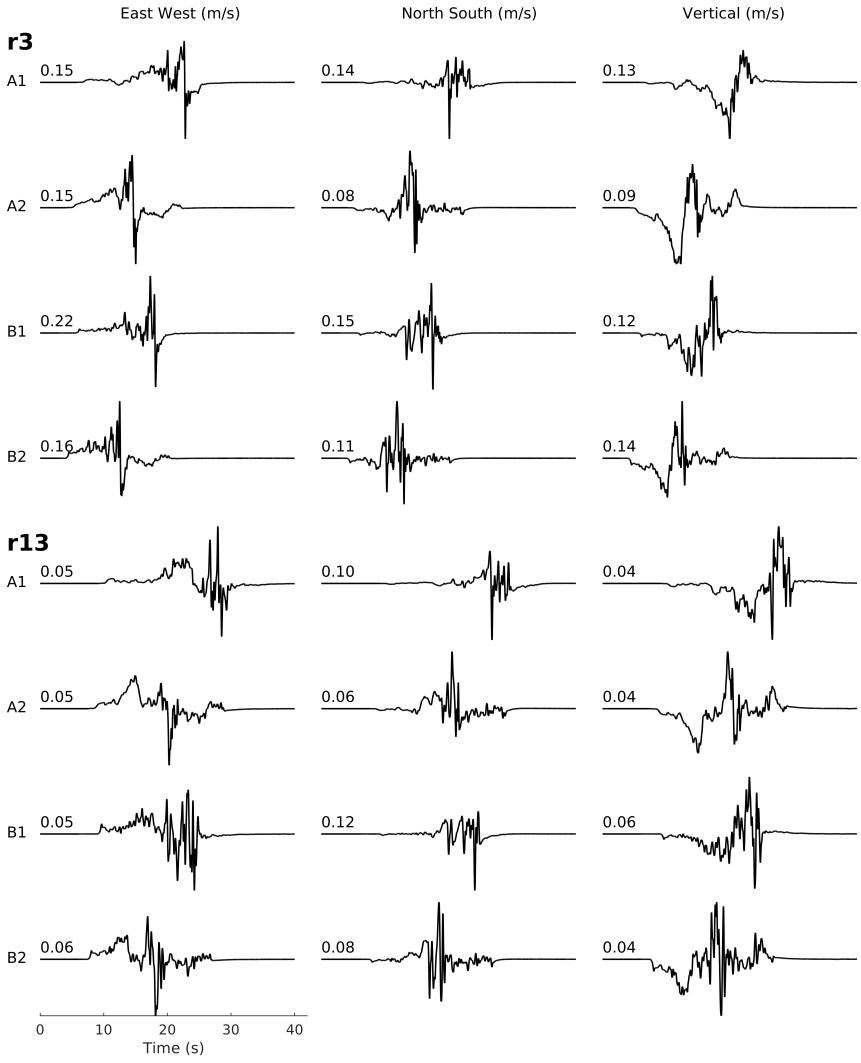

Figure S2: Ground velocity (m/s) for four selected rough fault models (A1, A2, B1, B2) at two stations (r3 and r13, see Figure 1). Waveforms are normalized to the absolute maximum of each trace (indicated in upper left corner).

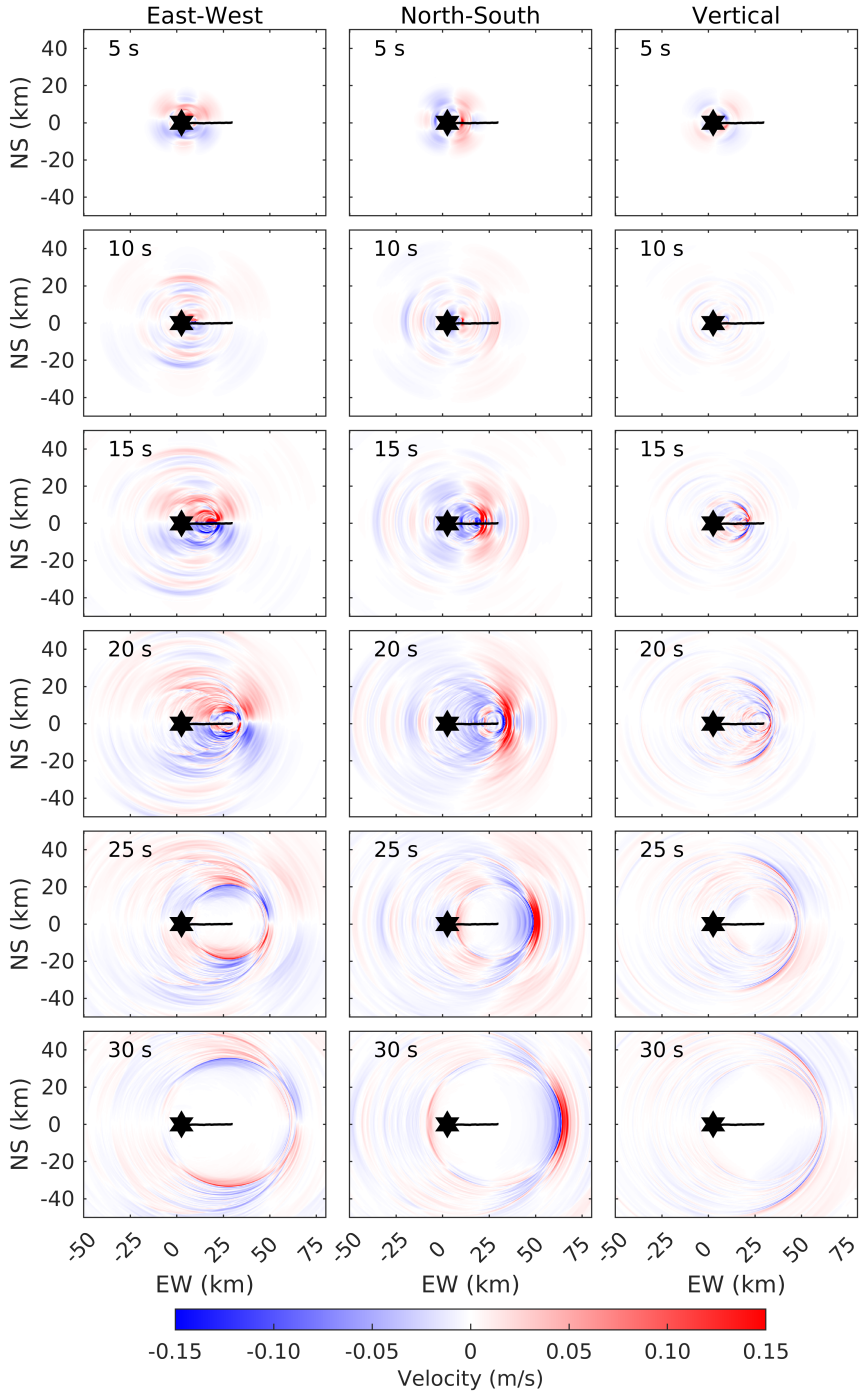

Figure S3: Snapshots of the east-west (EW), north-south (NS) and vertical (UD) components of ground-velocity (m/s) at the Earth surface for rupture model A1. The black star marks epicenter and black line is fault surface trace.

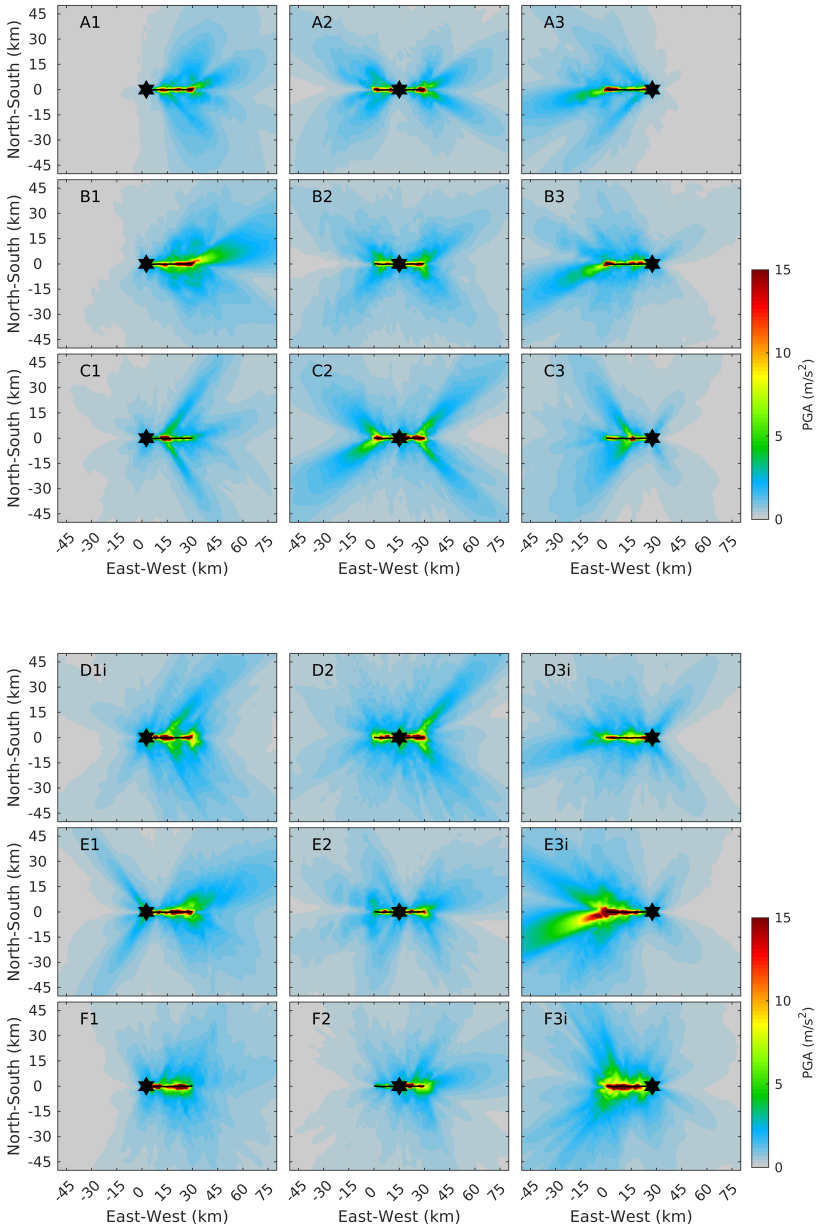

Figure S4: Spatial distribution of PGA at the Earth surface for all considered rupture models (see Table 2). The black star marks epicenter and black line is fault surface trace.

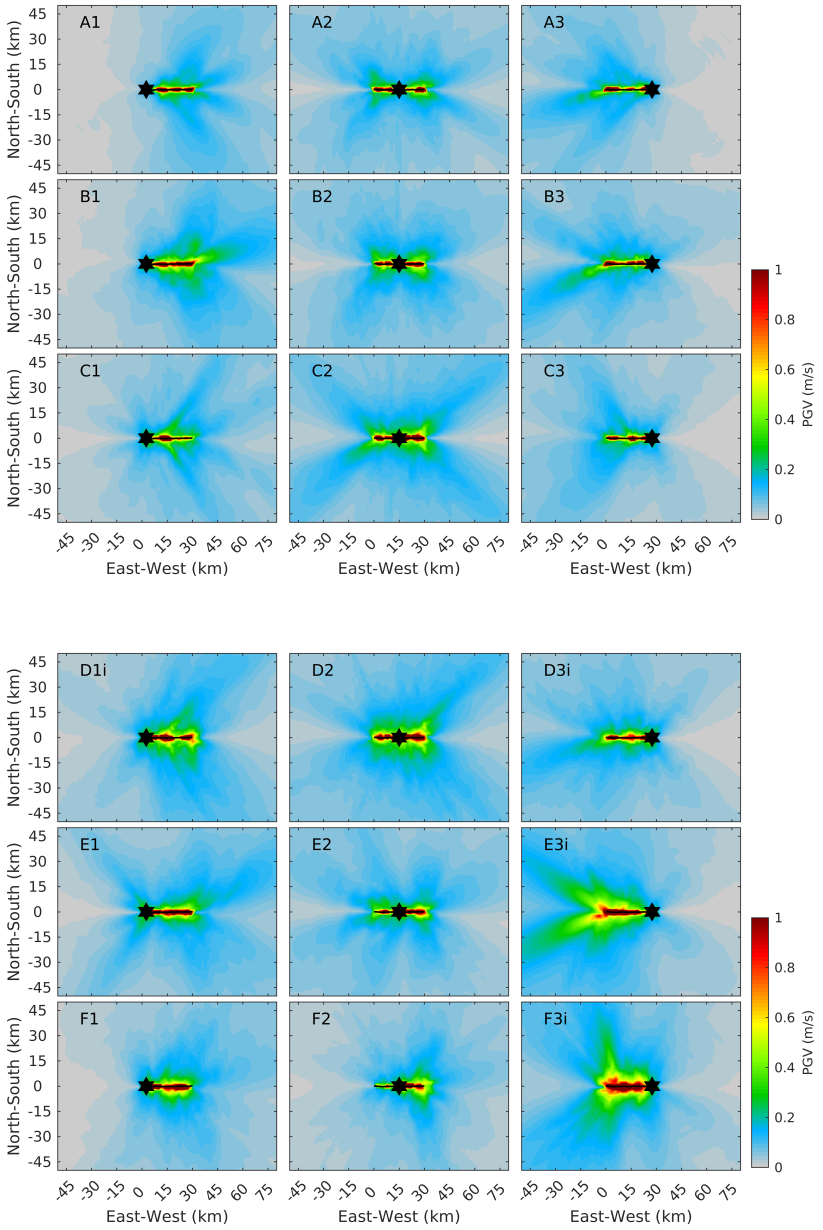

Figure S5: Shake-map like display of ground-motions (PGV) for eighteen rough fault models (see Table 2). The black star marks epicenter and black line is fault surface trace.

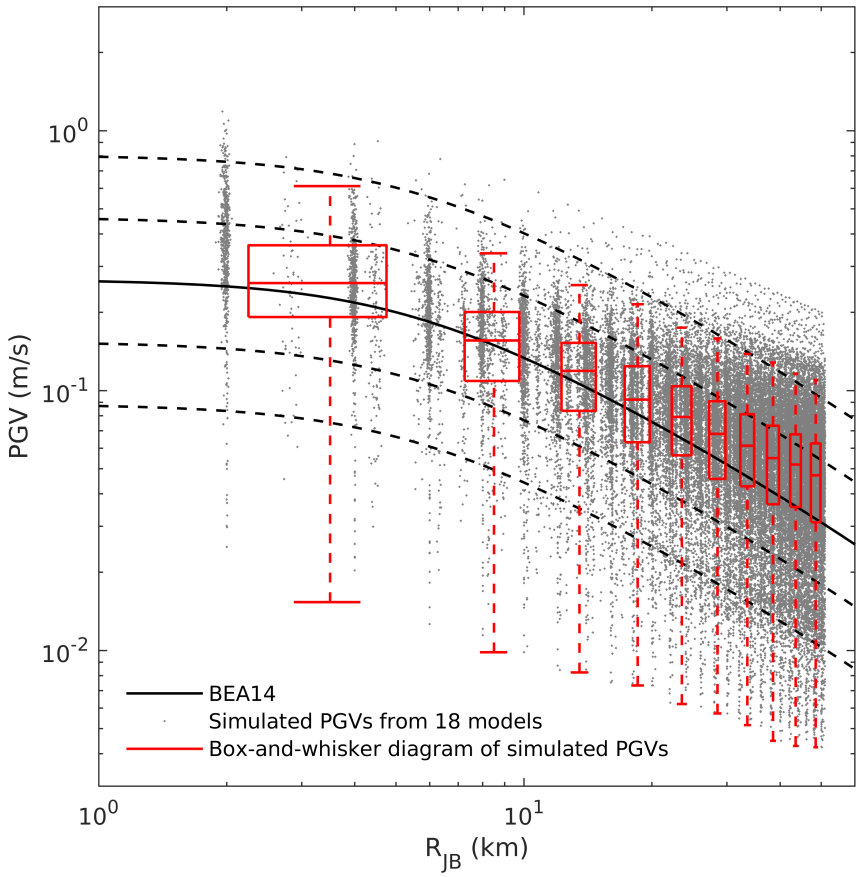

Figure S6: Comparison of PGV from rough-fault rupture simulations with estimates from empirical GMM (Boore et al., 2014; BEA14). The solid and dashed lines (black color) represent median, and one-and-two sigma bounds, respectively, of PGV from BEA14. Simulated PGVs (gray dots) are combined into ten R_{JB} distance bins (bin width 5 km) to generate box plots. In each box, central mark is median, bottom and top edges are representing 25^{th} and 75^{th} percentiles respectively of PGVs in each bin, whiskers indicate 1.5 times interquartile range.

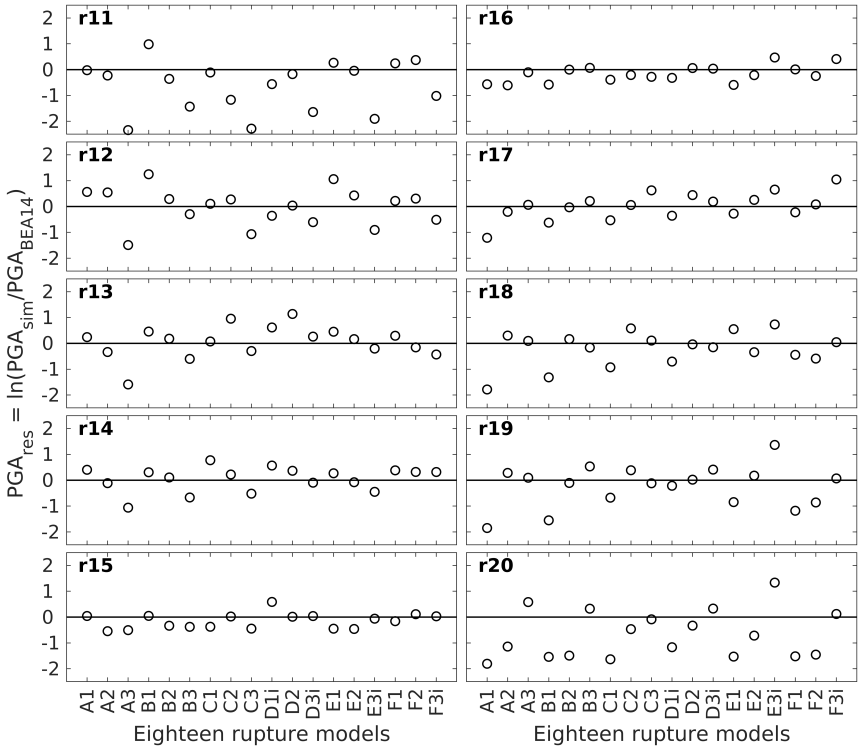

Figure S7: PGA residual (PGA_{res}) with respect to empirical GMM (Boore et al., 2014; BEA14) at receivers far from the fault (r11 to r20, see Figure 1).

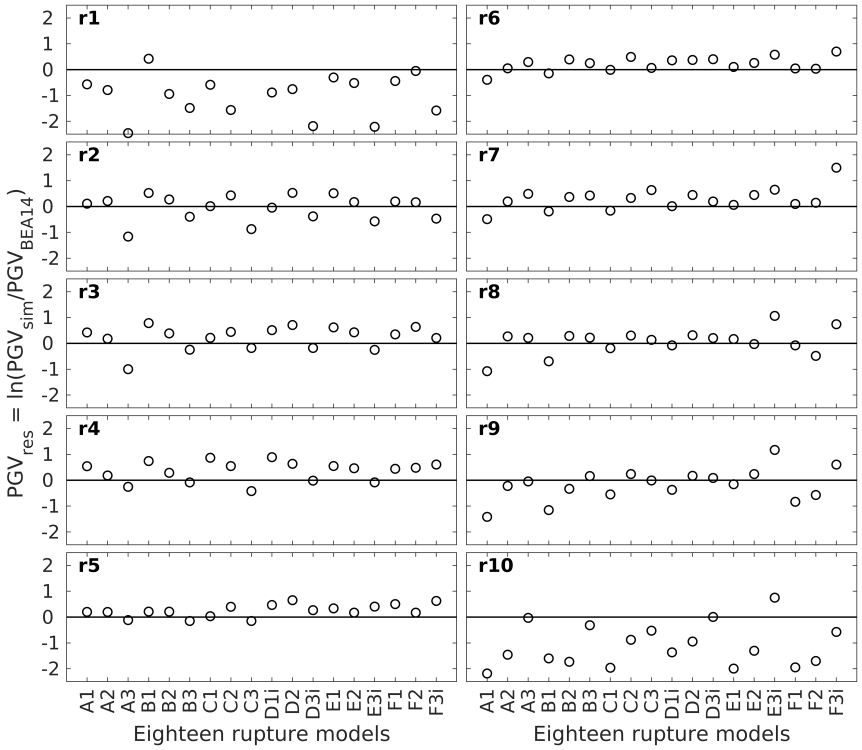

Figure S8: PGV residual (PGV_{res}) with respect to empirical GMM (Boore et al., 2014; BEA14) at receivers near the fault (r1 to r10, see Figure 1).

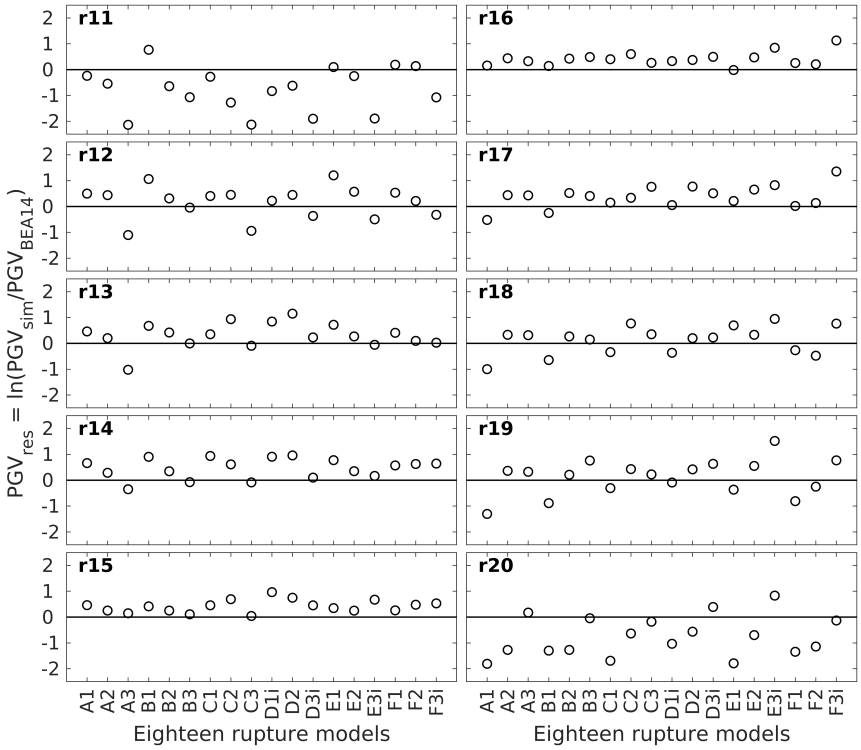

Figure S9: PGV residual (PGV_{res}) with respect to empirical GMM (Boore et al., 2014; BEA14) at receivers far from the fault (r11 to r20, see Figure 1).

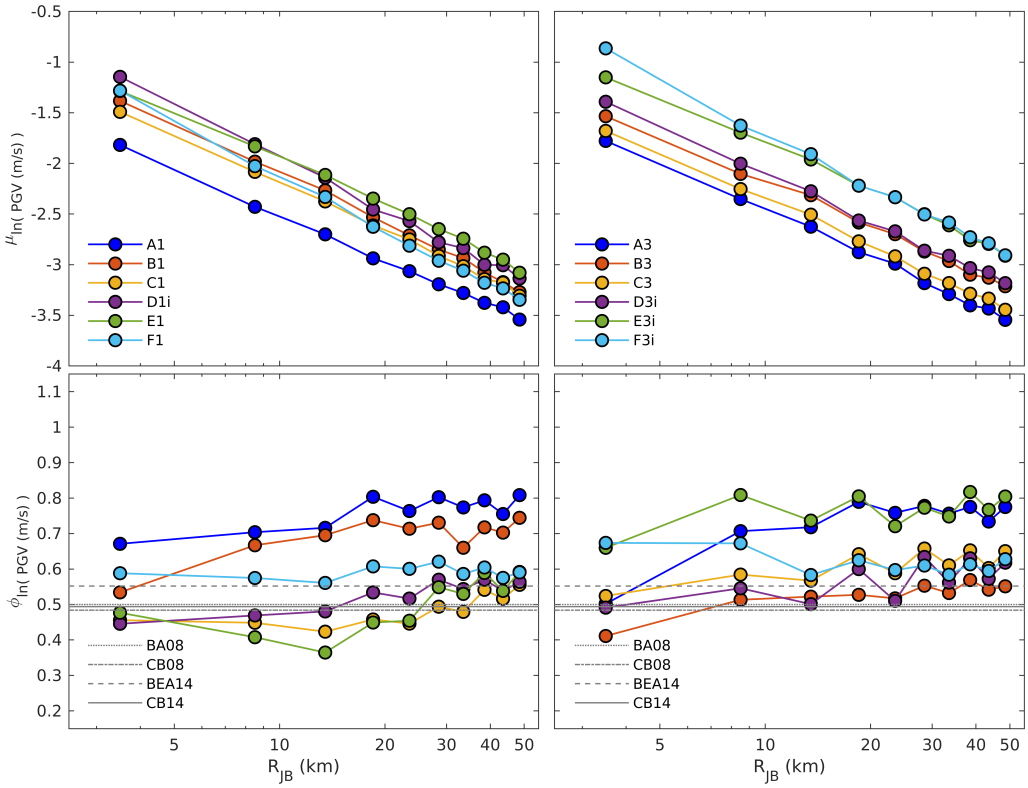

Figure S10: Distance dependence of the mean ($\mu_{ln(PGV)}$) and standard deviation ($\phi_{ln(PGV)}$) of $ln(PGV)$ for twelve unilateral dynamic rupture simulations. Note that indices 1 and 3 in model names indicate hypocentre location (see Figure 2). For clarity, we separate subplots for results for ruptures propagating towards right and left (indices 1 and 3, respectively). Abbreviations are as follows: BA08, Boore and Atkinson (2008); CB08, Campbell and Bozorgnia (2008); BEA14, Boore et al. (2014); and CB14, Campbell and Bozorgnia (2014).

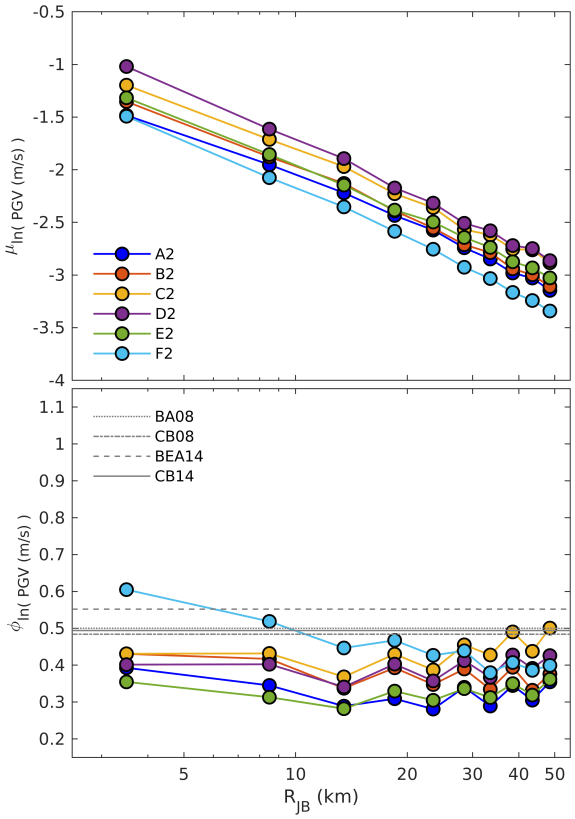

Figure S11: Distance dependence of the mean ($\mu_{ln(PGV)}$) and the standard deviation ($\phi_{ln(PGV)}$) of $ln(PGV)$ for six bilateral ruptures (see, Figure 2). Abbreviations follow Figure S10.

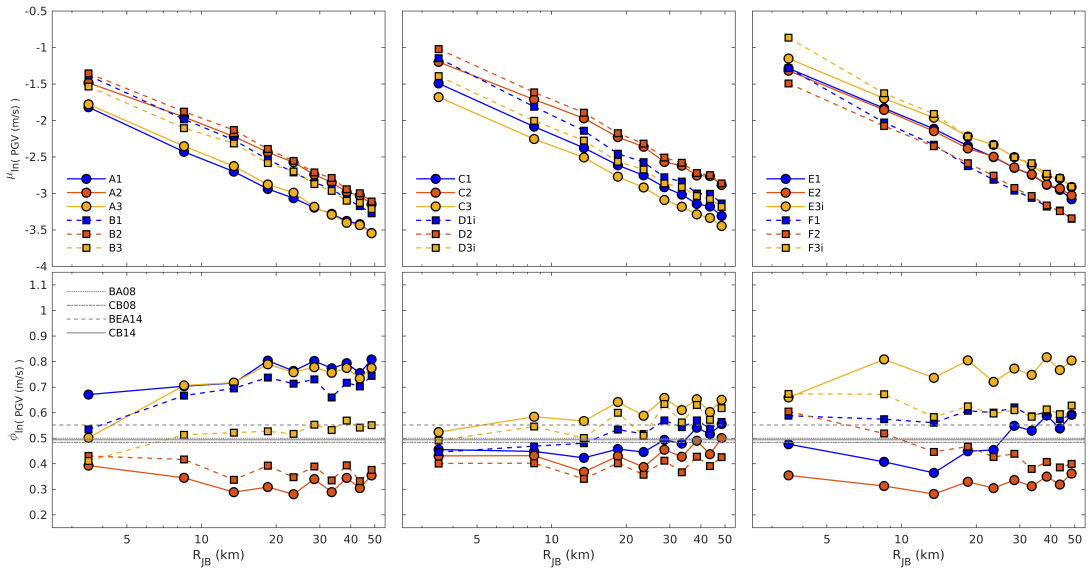

Figure S12: Effects of fault roughness on the mean ($\mu_{ln(PGV)}$) and standard deviation ($\phi_{ln(PGV)}$) of $ln(PGV)$ for all considered rupture models. The color indicates the realization of the spatial distribution of the fault roughness. The results for models with higher fault roughness are depicted by dashed lines and results for models models with lower roughness are depicted by solid lines. Abbreviations follow Figure S10.